Title

Differentiation of Cerebellar Hemisphere Tumors: Combining Apparent Diffusion Coefficient Histogram Analysis and Structural MRI Features

Journal

Journal of Neuroimaging, 28(6)

ISSN

1051-2284

Authors

Payabvash, Seyedmehdi
Tihan, Tarik
Cha, Soonmee

Publication Date

2018-11-01

DOI

10.1111/jon.12550

Peer reviewed

Original article

NRJ

The Neuroradiology Journal
2018, Vol. 31(6) 554–564

DOI: 10.1177/1971400918800803
journals.sagepub.com/home/neu
SAGE

Volumetric voxelwise apparent diffusion coefficient histogram analysis for differentiation of the fourth ventricular tumors

Seyedmehdi Payabvash[1,2], Tarik Tihan[3] and Soonmee Cha[1]

Abstract

Purpose: We applied voxelwise apparent diffusion coefficient (ADC) histogram analysis in addition to structural magnetic resonance imaging (MRI) findings and patients' age for differentiation of intraaxial posterior fossa tumors involving the fourth ventricle.

Participants and methods: Pretreatment MRIs of 74 patients with intraaxial brain neoplasm involving the fourth ventricle, from January 1, 2004 to December 31, 2015, were reviewed. The tumor solid components were segmented and voxelwise ADC histogram variables were determined. Histogram-driven variables, structural MRI findings, and patient age were combined to devise a differential diagnosis algorithm.

Results: The most common neoplasms were ependymomas ($n = 21$), medulloblastoma ($n = 17$), and pilocytic astrocytomas ($n = 13$). Medulloblastomas followed by atypical teratoid/rhabdoid tumors had the lowest ADC histogram percentile values; whereas pilocytic astrocytomas and choroid plexus papillomas had the highest ADC histogram percentile values. In a multivariable multinominal regression analysis, the ADC 10th percentile value from voxelwise histogram was the only independent predictor of tumor type ($p < 0.001$). In separate binary logistic regression analyses, the 10th percentile ADC value, tumor morphology, enhancement pattern, extension into Luschka/Magendie foramina, and patient age were predictors of different tumor types. Combining these variables, we devised a stepwise diagnostic model yielding 71% to 82% sensitivity, 91% to 95% specificity, 75% to 78% positive predictive value, and 89% to 95% negative predictive value for differentiation of ependymoma, medulloblastoma, and pilocytic astrocytoma.

Conclusion: We have shown how the addition of quantitative voxelwise ADC histogram analysis of the tumor solid component to structural findings and patient age can help with accurate differentiation of intraaxial posterior fossa neoplasms involving the fourth ventricle based on pretreatment MRI.

Keywords

Fourth ventricle, cerebellum, tumor, diffusion, histogram

Introduction

Currently, the presurgical neuroimaging of brain tumors is mainly aimed at establishing the differential diagnosis, determining the anatomical location and boundaries of the lesion(s), and identification of possible remote metastases throughout the neuroaxis. Although the histopathologic exam remains the gold standard for the diagnosis of brain tumors, surgical biopsies carry potential morbidity and mortality risks, and intraoperative microscopic diagnosis may have 3% to 8% error rates.[1] An accurate pretreatment neuroimaging diagnosis can help with treatment decisions such as the need for stereotactic biopsy vs complete resection, surgical planning as to whether the resection of a cystic component is necessary, or guiding potential neoadjuvant therapy prior to surgery.[2,3] Pretreatment neuroimaging can potentially reduce the number of patients requiring biopsy and tissue-based diagnosis by replacing histopathologic exam.

Radiological differentiation of posterior cranial fossa tumors can be challenging, particularly those localized to the fourth ventricle. Conventional magnetic

[1]Department of Radiology and Biomedical Imaging, Yale School of Medicine, New Haven, USA
[2]Department of Radiology and Biomedical Imaging, University of California, San Francisco, USA
[3]Department of Pathology, University of California, San Francisco, USA

Corresponding author:
Soonmee Cha, Department of Radiology and Biomedical Imaging, University of California, San Francisco, 350 Parnassus Ave., Box 0336, San Francisco, CA 94143-0336, USA.
Email: Soonmee.Cha@ucsf.edu

resonance imaging (MRI) findings such as the tumor morphology, enhancement pattern, or extension through the foramina of Luschka or Magendie tend to be helpful for the identification of tumor type, but can also be misleading.[4] For example, extension through the foramina of Luschka or Magendie is not exclusive to ependymomas, and can also be seen in patients with medulloblastomas. Also, pilocytic astrocytomas lacking typical cystic morphology with mural nodule can impose a diagnostic challenge.

Prior reports suggest that apparent diffusion coefficient (ADC) and diffusion-weighted imaging (DWI), can preoperatively predict the grade and type of brain tumors.[5] The ADC values of solid cerebellar tumors are related to tumor cellularity, and can help with differentiating and classifying posterior cranial fossa tumors.[2,3,6–8] However, prior studies have applied various methods for quantification of ADC properties of brain tumors with variable accuracy in their results.[2,3,6–8]

The purpose of our study was to analyze the volumetric voxelwise ADC histogram of solid components in intraaxial posterior fossa tumors involving the fourth ventricle, and apply the quantitative variables derived from ADC histogram analysis with other conventional imaging characteristics for differentiation of tumors based on pretreatment MRI.[9]

Methods

Patients

Using the surgical pathology database, we performed a retrospective review to identify all patients with a diagnosis of posterior fossa brain tumor involving the fourth ventricle from January 1, 2004 to December 31, 2015 at the University of California, San Francisco (UCSF). Patients were included if (1) the tumor was midline protruding or localized to the fourth ventricle based on presurgical MRI scan; (2) they had surgical pathology confirmation of a neoplasm, and (3) had presurgical MRI deemed adequate for image analysis. The MRI study was considered adequate if the ADC/DWI, T2, fluid-attenuated inversion recovery (FLAIR), and postcontrast T1 sequences were available and without substantial artifact. A total of 74 (18.1%) patients, with an average age of 25.4 ± 20.1 years, met the inclusion criteria for our study. The study protocol was reviewed for human participant protection and confidentiality and was approved by the UCSF institutional review board. Informed consent requirement was waived because of the retrospective nature of this study.

DWI technique

The MRI studies were performed on 1.5 or 3.0 Tesla MRI scanners. The most commonly used protocol/scanners were as follows: On GE Discovery MR750 3T scanner (Waukesha, WI), the acquisition protocol for the DWI series included an axial spin-echo echo-planar technique with a repetition time of 3600 ms, echo time of 107 ms, slice thickness of 2 mm, field of view of 240×240 mm, and acquisition matrix size of 128×128, with b values of 0 and 1000 seconds/mm^2; on the 1.5 Tesla GE Signa HD scanner (Waukesha, WI), the acquisition protocol for the DWI series included an axial spin-echo echo-planar technique with a repetition time of 9500 ms, echo time of 90 ms, section thickness of 2 mm, field of view of 250×250 mm, and matrix size of 128×128 with b values of 0 and 1000 seconds/mm^2.

MRI scan review and ADC histogram analysis

The MRI scans were reviewed on an AGFA IMPAX 6.5 (AGFA HealthCare, Mortsel, Belgium) by a neuroradiologist (S.P.) with six years of experience and blinded to the histological diagnosis of the lesions. The MRI findings were corroborated and confirmed according to the official clinical report. In case of discrepancy, the senior author (S.C.) with more than 25 years of experience reviewed the images to reach consensus.

The lesion morphology was categorized as predominantly solid (i.e. >80% of lesion), mixed solid and cystic, cystic (>80%) with smooth mural nodule, or cystic/necrotic (>80%) with irregular rim of enhancement based on visual assessment. The solid component enhancement was categorized as homogenous, heterogeneous, or none. The tumor locations were also categorized based on the presumable anatomical origin from the roof (superior aspect) vs the floor (inferior aspect) of the fourth ventricle. The presence of prominent vascular signal flow voids was determined on T2-weighted images and confirmed based on postcontrast T1 images. The maximum radial thickness of the surrounding T2 FLAIR hyperintensity on axial FLAIR sequences was determined. The solid component was categorized as T2 hyperintense when the signal intensity was higher than the gray matter, as described previously.[10]

For histogram analysis, the ADC maps were transferred to a GE Advantage Workstation (GE Healthcare, Milwaukee, WI). The solid component of the tumor was manually segmented based on ADC maps, with attention to postcontrast T1-weighted and T2-weighted images, by S.P. The voxelwise ADC histogram of the solid component volume was calculated and the ADC value percentiles with five percentile gaps were determined (e.g. minimum, 5th, 10th, 15th percentiles). We also calculated the ADC value mean, skewness, and kurtosis for the solid component. For each patient, the ADC values were normalized against the average ADC of cerebrospinal fluid in the body of lateral ventricles, which was set to 3400×10^{-6} mm^2/s.[11] Also, tumor volumes (including both cystic and solid components) were calculated on postcontrast T1 series based on manual segmentation.

Statistical analysis

The data are presented as average ± standard deviation, and proportion (percentage). The Kolmogorov-Smirnov test confirmed normal distribution of continuous variables (i.e. patient age, tumor volume, and ADC histogram variables); thus, we used analysis of variance (ANOVA) with Tukey *b* post-hoc analysis to compare continuous variables among different tumor types. For the nominal variables, chi-squared test was used. Stepwise multivariable multinominal regression analysis was used to identify the independent predictor(s) for differentiation of tumor types among ADC metrics and structural findings. To develop the differential diagnosis algorithm, separate stepwise binary logistic regressions were applied for classification of each tumor type. For stepwise regression analysis, the forward likelihood ratio selection method was applied—the likelihood ratio probability p value for variables entry was set to 0.05, and for variable removal to 0.10. Dichotomization of continuous variables was based on the operating point values determined via receiver operating characteristic (ROC) analysis. In addition, area under the curve (AUC) of ROC was determined as a measure of test accuracy. All statistical analyses were performed using SPSS 22.0 (SPSS, IBM, Somers, NY). A p value < 0.05 was considered statistically significant.

Results

Tumor pathological characteristics

The final pathological diagnoses for the patients are listed in Table 1. Among 74 patients, 11 different types of tumors were identified. Ependymomas, medulloblastomas, and pilocytic astrocytomas were the three most common fourth-ventricular tumors.

Table 1. Pathological diagnoses of fourth-ventricular tumors.

Diagnosis	Patients Number (proportion)
Ependymoma	21 (28.4%)
Medulloblastoma	17 (23%)
Pilocytic astrocytoma	13 (17.6%)
Subependymoma	6 (8.1%)
Choroid plexus papilloma	4 (5.4%)
Atypical teratoid/rhabdoid tumor	4 (5.4%)
Hemangioblastoma	3 (4.1%)
Metastasis	3 (4.1%)
Lymphoma	1 (1.4%)
Rosette-forming glioneuronal tumor	1 (1.4%)
Neurocytoma	1 (1.4%)
Total	74 (100%)

Imaging characteristics of the fourth-ventricular tumors

There was a significant difference in average age of patients among different tumor types (Table 2). In the post hoc analysis, patients with subependymoma had significantly higher average age compared to those with pilocytic astrocytoma ($p = 0.006$), medulloblastoma ($p < 0.001$), ependymoma ($p = 0.005$), and atypical teratoid/rhabdoid tumors (ATRT, $p < 0.001$). Also, patients with metastasis were older (61.5 ± 5.2 years) compared to those with pilocytic astrocytoma ($p = 0.003$), medulloblastoma ($p < 0.001$), ependymoma ($p = 0.003$), and ATRT ($p < 0.001$). In addition, patients with ATRT were significantly younger than those with hemangioblastoma ($p = 0.014$) and choroid plexus papilloma ($p = 0.046$).

There was significant difference in tumor morphology among different histopathology types (Table 2): All subependymomas, metastases, and choroid plexus papillomas presented with a predominantly (>80%) solid component, whereas only a few pilocytic astrocytomas (15%) and hemangioblastomas (33%) had predominantly solid morphology ($p = 0.005$).

With regards to extension of the tumors through the foramina of Luschka/Magendie, the majority of ependymomas (81%), choroid plexus papillomas (75%), pilocytic astrocytomas (69%), and subependymomas (67%) showed extension through the fourth-ventricular outflow tracks ($p = 0.024$). Notably, 35% of medulloblastomas also extended into the foramina of Luschka/Magendie.

When analyzing the enhancement pattern, the majority of choroid plexus papillomas (75%) and hemangioblastomas (67%) had homogenous enhancement, while the rest of the tumors predominantly had heterogeneous or no enhancement ($p = 0.001$, Table 2). There were also significant differences in the presence of prominent vascular flow void, T2 hyperintense solid component, and hydrocephalus among various tumor types (Table 2).

ADC histogram analysis

There was significant difference in ADC percentile values ($p < 0.001$), skewness ($p = 0.006$), and average ($p < 0.001$) between different tumor types on ANOVA analysis. Figure 1(a) demonstrates the schematic representation of the averaged ADC percentile values among the fourth-ventricular tumors with $n > 3$. The average of median ADC values ($\times 10^{-6}\,mm^2/s$) were 721.1 ± 175.6 for medulloblastomas, 1243.7 ± 335.4 for ependymomas, 1253.8 ± 303.4 for subependymomas, and 1896.8 ± 369.6 for pilocytic astrocytomas (Figure 1(b)). The solid component of medulloblastomas followed by ATRT showed the lowest ADC percentile values; on the other end of spectrum, pilocytic astrocytomas and then choroid plexus papillomas had the highest ADC percentile values (Figure 1). Ependymomas and subependymomas demonstrate

Table 2. Imaging and clinical characteristics of fourth-ventricular tumors.

	EP ($n=21$)	MB ($n=17$)	PA ($n=13$)	SEP ($n=6$)	CPP ($n=4$)	ATRT ($n=4$)	Mets ($n=3$)	HB ($n=3$)	p value
Age	22.4 ± 19.6	14.9 ± 13.2	21.1 ± 11.7	50.2 ± 13.3	36.1 ± 11.2	1.8 ± 0.9	61.5 ± 5.3	43.9 ± 25.5	<**0.001**
Gender (male)	10 (48%)	9 (53%)	6 (46%)	3 (50%)	0 (0%)	2 (50%)	1 (33%)	1 (33%)	0.756
Lesion morphology									
Predominantly solid	11 (52%)	11 (65%)	2 (15%)	6 (100%)	4 (100%)	2 (50%)	3 (100%)	1 (33%)	**0.005**
Mixed solid and cystic	10 (48%)	6 (35%)	7 (54%)	0 (0%)	0 (0%)	2 (50%)	0 (0%)	1 (33%)	0.157
Cystic with mural nodule	0 (0%)	0 (0%)	2 (15%)	0 (0%)	0 (0%)	0 (0%)	0 (0%)	1 (33%)	0.080
Cystic with irregular wall	0 (0%)	0 (0%)	2 (15%)	0 (0%)	0 (0%)	0 (0%)	0 (0%)	0 (0%)	0.240
Foraminal extension[a]	17 (81%)	6 (35%)	9 (69%)	4 (67%)	4 (75%)	1 (25%)	0 (0%)	1 (33%)	**0.024**
Homogenous enhancement	0 (0%)	4 (24%)	1 (8%)	1 (17%)	3 (75%)	0 (0%)	0 (0%)	2 (67%)	**0.001**
Origin from ventricle floor	19 (91%)	9 (53%)	10 (77%)	5 (83%)	4 (100%)	2 (50%)	1 (33%)	3 (100%)	0.058
Prominent vessel flow void	3 (14%)	6 (35%)	0 (0%)	0 (0%)	0 (0%)	1 (33%)	0 (0%)	2 (67%)	**0.036**
Leptomeningeal metastasis	0 (0%)	1 (6%)	1 (8%)	0 (0%)	0 (0%)	0 (0%)	1 (33%)	0 (0%)	0.294
Volume (solid + cystic, ml)	23.4 ± 18.7	30.4 ± 23.2	24.2 ± 22.4	11.9 ± 15.7	13.9 ± 11.2	41.4 ± 37.4	7.7 ± 6.7	4.5 ± 4.4	0.079
Hydrocephalus	16 (76%)	14 (82%)	10 (77%)	0 (0%)	2 (50%)	4 (100%)	1 (33%)	3 (100%)	**0.003**
T2-hyperintense tumor[b]	9 (43%)	4 (24%)	10 (77%)	0 (0%)	2 (50%)	0 (0%)	2 (67%)	1 (33%)	**0.016**

ATRT: atypical teratoid/rhabdoid tumors; CPP: choroid plexus papilloma; EP: ependymoma; HB: hemangioblastoma; MB: medulloblastoma; Mets: metastasis; PA: pilocytic astrocytoma; SEP: subependymoma.
[a]Lesion extension through the foramina of Luschka and/or Magendie.
[b]Solid component T2-signal higher than gray matter.[10]

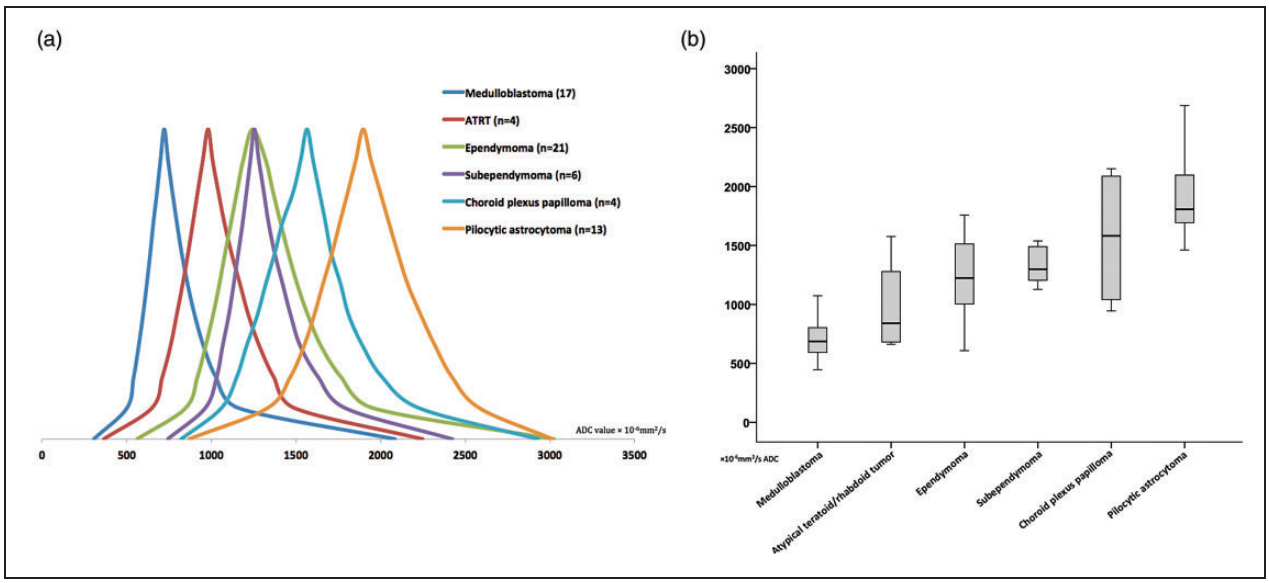

Figure 1. (a) Schematic representation of the averaged ADC histogram value distribution among fourth-ventricular tumors (with $n > 3$). On the Y axis, the histogram representations were modified so the median values would have the same heights across different tumor types. (b) The average (95% confidence interval) distribution of voxelwise median ADC values of the solid component among different fourth-ventricular tumors. ADC: apparent diffusion coefficient; ATRT: atypical teratoid/rhabdoid tumors.

similar ADC histogram values with ADC percentile distribution in the midspectrum among the fourth-ventricular tumors (Figure 1).

Differentiation of fourth-ventricular tumors

Among all ADC histogram as well as imaging variables listed in Table 2, the 10th percentile ADC value was the only independent predictor of tumor type among medulloblastomas, pilocytic astrocytomas, and ependymomas in a multivariable multinominal regression analysis (Table 3, $p < 0.001$).

In separate binary logistic regression analyses, the independent predictors for different fourth-ventricular tumors were identified (Tables 4–8). The regression model could not resolve statistically significant

Table 3. Multivariable multinominal regression analysis for identification of independent predictor(s) differentiating fourth-ventricular medulloblastoma, pilocytic astrocytoma, and ependymoma.

Pathology	Predictor	*B* coefficient	Odds ratio (95% confidence interval)	*p* value
Pilocytic astrocytoma	ADC 10th percentile	0.013	1.013 (1.002–1.025)	0.022
	Intercept	−15.887		0.021
Medulloblastoma	ADC 10th percentile	−0.014	0.986 (0.977–0.996)	0.004
	Intercept	9.269		0.003
The reference category is ependymoma.				

ADC: apparent diffusion coefficient.
In stepwise multivariable multinominal regression analysis for differentiation of fourth-ventricular medulloblastoma, pilocytic astrocytoma, and ependymoma ($n = 51$), ADC 10th percentile value was the only independent predictor ($p < 0.001$ for whole regression model).

Table 4. Multivariable binary logistic regression analysis for identification of independent predictor(s) of fourth-ventricular medulloblastoma.

Predictor	*B* coefficient	Odds ratio (95% confidence interval)	*p* value
ADC 10th percentile	−0.009	0.991 (0.986–0.996)	<0.001
Intercept	5.385		0.001

ADC: apparent diffusion coefficient.
In stepwise multivariable binary logistic regression analysis for differentiation of fourth-ventricular medulloblastoma, ADC 10th percentile value was the only independent predictor ($p < 0.001$ for whole regression model).

Table 5. Multivariable binary logistic regression analysis for identification of independent predictor(s) of fourth-ventricular pilocytic astrocytoma.

Predictor	*B* coefficient	Odds ratio (95% confidence interval)	*p* value
ADC 10th percentile	0.005	1.005 (1.002–1.008)	0.001
Presence of cystic component (>20%)	2.252	9.509 (1.371–65.966)	0.023
Intercept	−8.662		<0.001

ADC: apparent diffusion coefficient.
In stepwise multivariable binary logistic regression analysis for differentiation of fourth-ventricular pilocytic astrocytoma, ADC 10th percentile value and presence of cystic component were the only independent predictors ($p < 0.001$ for whole regression model).

Table 6. Multivariable binary logistic regression analysis for identification of independent predictor(s) of fourth-ventricular ependymoma.

Predictor	*B* coefficient	Odds ratio (95% confidence interval)	*p* value
Heterogeneous enhancement pattern	20.773	1.512 (1.265–1.807)	0.001
Extension through Luschka/Magendie	0.64	1.896 (1.194–3.011)	0.002
Intercept	−22.366		<0.001

In stepwise multivariable binary logistic regression analysis for differentiation of fourth-ventricular ependymoma, heterogeneous enhancement pattern and extension through the Luschka/Magendie foramina were the only independent predictors ($p < 0.001$ for whole regression model).

predictors for the rest of the tumors. Based on these results, a stepwise differentiation algorithm was developed (Figure 2).

The 10th percentile ADC value was the only independent predictor of medulloblastoma (Table 4, $p < 0.001$). In the first step of the proposed differentiation algorithm, the 10th percentile ADC value had an ROC AUC of 0.877 (95% CI: 0.763–0.99, $p < 0.001$) for differentiation of medulloblastoma from other fourth-ventricular tumors, with a 10th percentile ADC value $< 580 \times 10^{-6}\,mm^2/s$ as an operating point yielding 82% sensitivity and 93% specificity (Figure 2).

For pilocytic astrocytoma, the 10th percentile ADC value ($p = 0.001$) and nonsolid morphology (>20%

Table 7. Multivariable binary logistic regression analysis for identification of independent predictor(s) of fourth-ventricular subependymoma.

Predictor	*B* coefficient	Odds ratio (95% confidence interval)	*p* value
Patients' age	0.072	1.075 (1.019–1.134)	0.008
Intercept	−5.108		<0.001

In stepwise multivariable binary logistic regression analysis for differentiation of fourth-ventricular subependymoma, patient age was the only independent predictor ($p = 0.002$ for whole regression model).

Table 8. Multivariable binary logistic regression analysis for identification of independent predictor(s) of fourth-ventricular hemangioblastoma.

Predictor	*B* coefficient	Odds ratio (95% confidence interval)	*p* value
Homogenous enhancement pattern	2.501	12.2 (1.01–147.42)	0.049
Intercept	−4.111		<0.001

In stepwise multivariable binary logistic regression analysis for differentiation of fourth-ventricular hemangioblastoma, homogenous enhancement pattern was the only independent predictor ($p = 0.044$ for whole regression model).

cystic component, $p = 0.023$) were independent predictors in binary logistic regression (Table 5, $p < 0.001$). In the second step of the proposed differentiation algorithm, a 10th percentile ADC value $\geq 1100 \times 10^{-6}\,mm^2/s$ (operating point) and presence of cystic component yielded an ROC AUC of 0.85 (95% CI: 0.706–0.993, $p < 0.001$) for differentiation of pilocytic astrocytoma from fourth-ventricular tumors not fulfilling step 1 (Figure 2).

For ependymomas, the heterogeneous enhancement pattern ($p = 0.001$) and extension through the Luschka/Magendie foramina ($p = 0.002$) were independent predictors in binary logistic regression (Table 6, $p < 0.001$). In the third step of the proposed differentiation algorithm, the presence of heterogeneous enhancement and extension through the foramina of Luschka/Magendie yielded an ROC AUC of 0.817 (95% CI: 0.681–0.953, $p < 0.001$) for differentiation of ependymomas from fourth-ventricular tumors in remaining participants (Figure 2).

In binary logistic regression, patient age and homogenous enhancement pattern were also independent predictors for subependymomas and hemangioblastomas, respectively (Tables 7 and 8). However, the total number of participants was too small to draw a firm conclusion (Figure 2). Notably, patient age yielded an ROC AUC of 0.868 (95% CI: 0.767–0.968, $p = 0.003$) for differentiation of subependymoma with age > 45 years (operating point) having 83% sensitivity and 84% specificity.

Discussion

Our results demonstrate how voxelwise ADC histogram analysis of solid components can help with differentiation of intraaxial cerebellar tumors involving the fourth ventricle. Overall, medulloblastomas followed by ATRT had the lowest ADC histogram percentile values reflecting the compact cellularity of these tumors.[3] On the other hand, pilocytic astrocytomas demonstrate the highest level of diffusibility, presumably related to abundant myxoid stroma.[7] Among ADC histogram and imaging variables, the 10th percentile ADC histogram value of tumor solid component was the only independent predictor of tumor type in multivariate multinominal regression analysis. We also devised a stepwise diagnostic algorithm combining voxelwise ADC histogram analysis and structural MRI findings for pretreatment differentiation of fourth-ventricular tumors, with an ROC AUC of 0.817 to 0.877 for identification of the three most common tumor types: ependymoma, medulloblastoma, and pilocytic astrocytoma.

Specifically, our findings suggest that the first step in formulating the differential diagnosis for fourth-ventricular tumors should be attention to the diffusion characteristics of the solid component on DWI/ADC sequence (Figures 2 and 3). Also, voxelwise ADC histogram analysis of the solid component can provide an objective and quantitative measure for differentiation of these tumors. Figure 3 provides examples of fourth-ventricular tumors, which can be challenging to diagnose based on conventional imaging findings, given that these three tumors extended into the foramen of Luschka. However, the solid component appearance on DWI/ADC and the 10th percentile ADC values can help with accurate differentiation on presurgical MRI. These examples demonstrate how conventional MRI findings can be misleading, particularly in our cohort: 35% of medulloblastomas and 69% of pilocytic astrocytomas showed extension through the foramina of Luschka/Magendie, which is classically described for ependymomas. Accordingly, we have shown that attention to ADC values can rule out or rule in the diagnosis

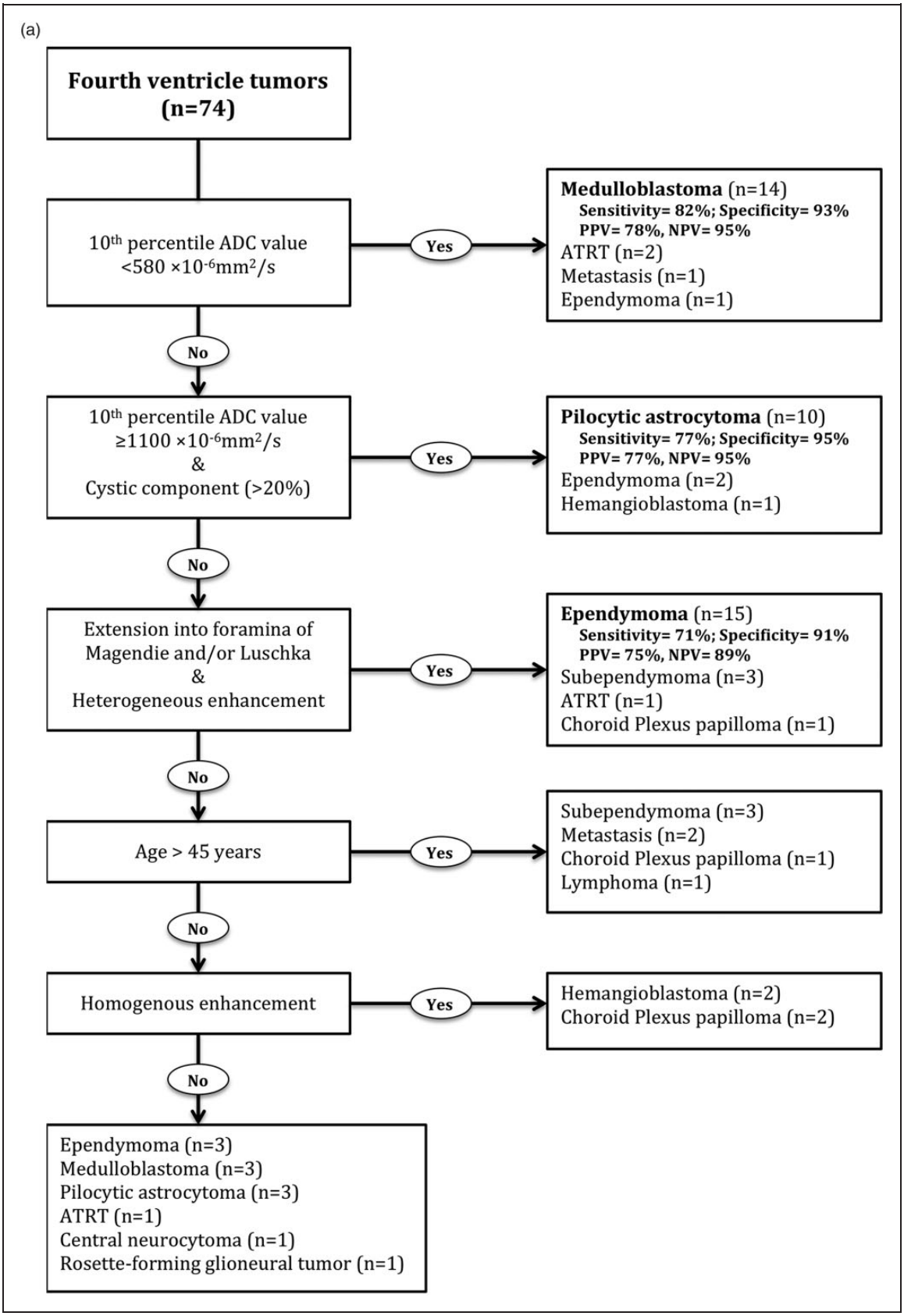

Figure 2. (a) Stepwise algorithm for differentiation of fourth-ventricular tumors. The test characteristics reported in the right-side column were determined among remaining patients at each step. For example, in the second step, a 10th percentile ADC value $\geq 1100 \times 10^{-6}$ mm^2/s and presence of cystic component could identify 10 pilocytic astrocytomas among 56 remaining patients from those in the first step, who did not fulfill the criteria for a 10th percentile ADC value $< 580 \times 10^{-6}$ mm^2/s. (b) From top to bottom, the ROC analysis for differentiation of medulloblastoma, pilocytic astrocytoma, and ependymoma in steps 1 to 3 of the proposed differentiation algorithm (a).

95% CI: 95% confidence interval; ADC: apparent diffusion coefficient; ATRT: atypical teratoid/rhabdoid tumors; NPV: negative predictive value; PPV: positive predictive value; ROC: receiver operating characteristics.

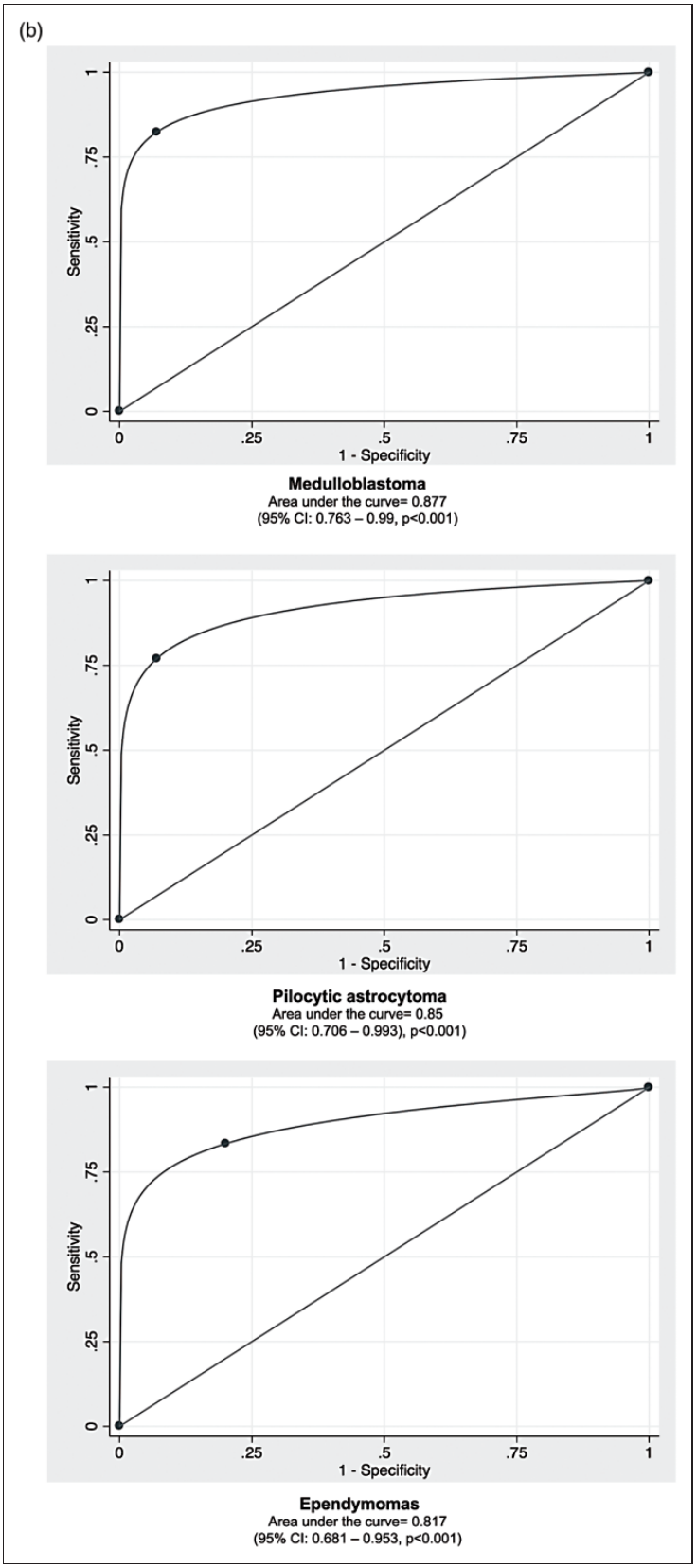

Figure 2. Continued.

of medulloblastoma and pilocytic astrocytoma at the first two steps of the differentiation algorithm, with priority over the presence of transforaminal extension (Figure 2).

The stepwise differential diagnosis algorithm proposed for fourth-ventricular tumors combines the ADC histogram analysis with patient age and other imaging findings such as tumor morphology, extension

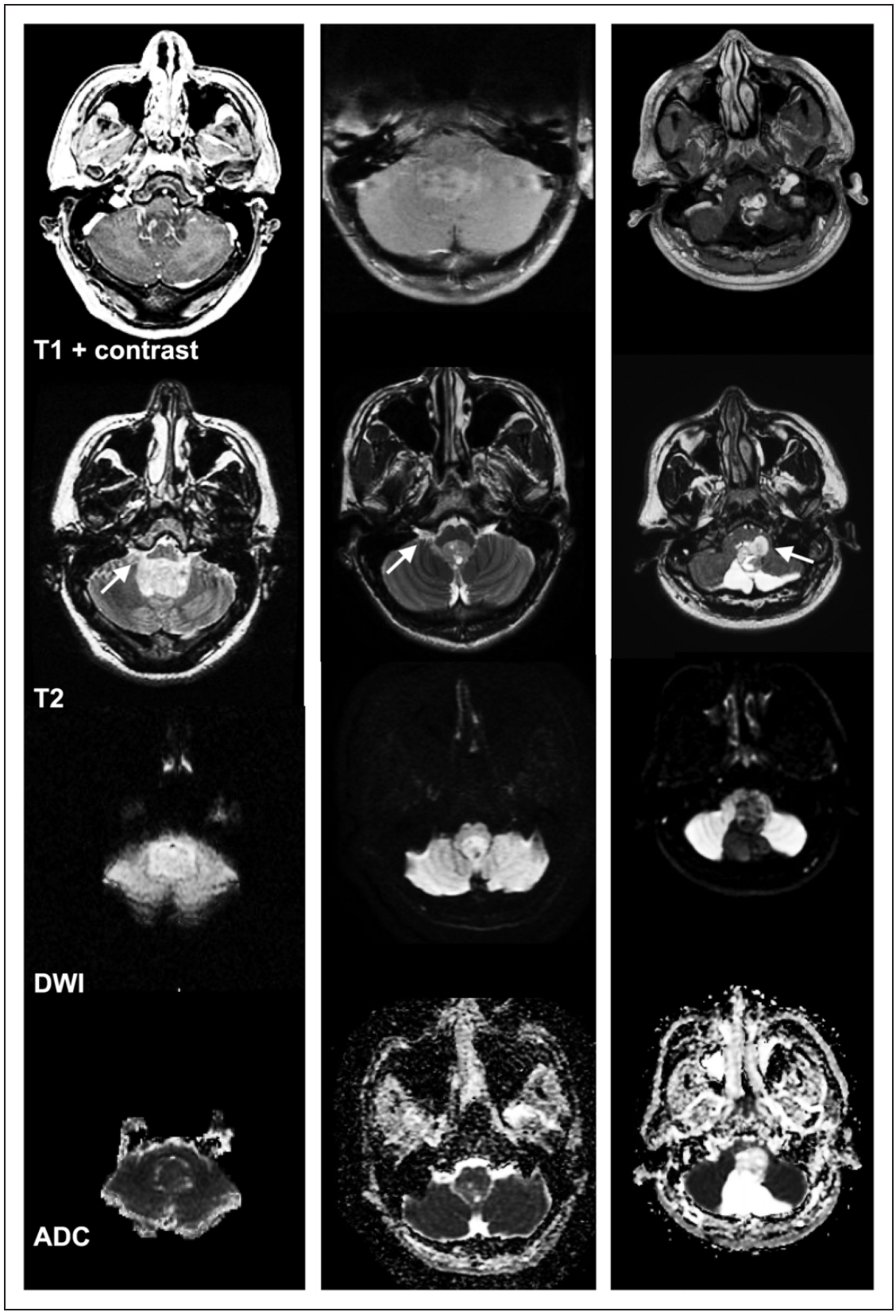

Figure 3. Application of DWI and ADC histogram analysis for differentiation of fourth-ventricular tumors. Examples of three different fourth-ventricular tumors extending into the foramen of Luschka (arrows). The left column depicts a medulloblastoma with a 10th percentile ADC value of $568 \times 10^{-6}\,mm^2/s$, the central column displays an ependymoma with a 10th percentile ADC value of $874 \times 10^{-6}\,mm^2/s$, and the right column shows a pilocytic astrocytoma with a 10th percentile ADC value of $1487 \times 10^{-6}\,mm^2/s$. The rows from top to bottom demonstrate postcontrast T1, T2, DWI, and ADC sequences. ADC: apparent diffusion coefficient; DWI: diffusion-weighted imaging.

into foramina of Luschka/Magendie, and enhancement pattern (Figure 2). While many of these features have previously been suggested for distinguishing specific types of posterior cranial fossa tumors,[4,12] we have combined these imaging characteristics with quantitative ADC histogram analysis to formulate a diagnostic approach. At the first step, a fourth-ventricular tumor with reduced diffusion, specifically with a voxelwise 10th percentile ADC value $< 580 \times 10^{-6}\,mm^2/s$, most likely represents a medulloblastoma. On the other hand, if the solid component demonstrates very high diffusivity instead of very low diffusivity, the tumor might be a pilocytic astrocytoma. In the second step of the diagnostic algorithm, tumors with a 10th percentile ADC value $\geq 1100 \times 10^{-6}\,mm^2/s$ and >20% cystic component on visual assessment were most likely pilocytic astrocytomas. After excluding very low and very high ADC values in the solid component of tumor (corresponding to medulloblastoma and pilocytic astrocytoma, respectively), one can consider ependymoma in differential diagnosis. In the third step, among those tumors not fulfilling the ADC histogram criteria for medulloblastoma or pilocytic astrocytoma, the presence of foramina extension and heterogeneous enhancement pattern are suggestive of ependymoma. Differentiation of less common tumors remains challenging. Nevertheless, in those cases not fulfilling the aforementioned criteria, older age (>45 years old) raises the possibility of subependgymoma and metastases, whereas homogenous enhancement may suggest hemangioblastomas and choroid plexus papillomas.

Quantitative assessment of ADC maps has shown potential for presurgical differentiation of posterior cranial fossa tumors.[7,8,12,13] Prior studies have applied various methods to measure water diffusivity in tumors based on ADC maps, and were promising for differentiation of brain tumors; however, some of these studies have produced conflicting results.[3,6–8,12–15] Some studies have limited their analysis to minimum, average, quartile, median ADC values, or the normalized ADC values within the tumor.[3,6–8,12–15] Also, some studies have limited ADC assessment to one (or multiple) region(s) of interests or the enhancing component instead of the whole tumor volume.[3,6–8,12–15] In the current study, we determined the voxelwise ADC histogram metrics in the entire solid volume of each fourth-ventricular tumor. Such analysis provides a more comprehensive assessment of the entire tumor cellularity and allows for the comparison of different ADC histogram derivatives for tumor type differentiation. In addition, we did not restrict the inclusion criteria to a certain tumor type, which may provide a more realistic assessment for the statistical test characteristics of the proposed differentiation algorithm.

Recently, there has been an increasing interest in the application of machine learning analysis to combine multiple imaging features for differentiation of brain tumors, distinguishing tumor progression from posttreatment changes, and prediction of patient survival.[12] Rodriguez Gutierrez et al. have combined metrics derived from tumor shape, morphology, and ADC histogram to train support vector machines for classification of the major pediatric posterior cranial fossa tumors.[12] Their study included 40 children with medulloblastomas, pilocytic astrocytomas, and ependymomas; and an average of 91.4% correct classification was achieved for these three tumor types, combining the 25th percentile, 75th percentile, and skewness in ADC histogram.[12] While machine-learning classification methods appear to be the de facto next step in development of multivariable differential diagnosis models, they demand a large number of patients to achieve enough statistical power for producing meaningful classifiers.

Similar to many other neuroimaging studies of brain tumors, our study is a retrospective analysis of imaging and pathological correlation. The small number of patients with less-common tumor types and uneven samples size were among limitations of our study. Another potential limitation is MRI acquisition in two different field strengths and on various scanners, though this should not substantially affect ADC values obtained with repetition time >3000 ms and *b* value of 1000 sec/mm^2.[16] Manual segmentation of the solid segments of tumor and visual assessment of the tumor morphology can limit the generalization of the results. In addition, the ADC maps were not coregistered and resliced before segmentation. There was also no assessment for interobserver agreement given that the study design was primarily based on image review and lesion segmentation by one neuroradiologist. Unfortunately, no measure of histological cellularity was available in our study; however, it would have been desirable to correlate ADC values of tumors with their cellularity as obtained from histopathology.

Conclusion

Our study demonstrates the diagnostic value of voxelwise volumetric ADC histogram analysis in differentiating various posterior fossa tumors involving the fourth ventricle. Quantitative metrics derived from the ADC histogram analysis can help with accurate classification of the three most common fourth-ventricular tumors, especially in the pediatric population. Combination of the ADC histogram analysis and conventional imaging features can be applied to devise a diagnostic algorithm for pretreatment differentiation of tumors and guide treatment decisions and surgical planning. Future work with larger samples and prospective studies can potentially produce more statistically powerful classification models.

Acknowledgment

Parts of these data were presented at the 55th annual American Society of Neuroradiology meeting, April 24–27, 2017, in Long Beach, CA.

Funding

This research received no specific grant from any funding agency in the public, commercial, or not-for-profit sectors.

Conflict of interest

The authors declared no potential conflicts of interest with respect to the research, authorship, and/or publication of this article.

ORCID iD

Seyedmehdi Payabvash http://orcid.org/0000-0003-4628-0370

References

1. Winkler D, Lindner D, Richter A, et al. The value of intraoperative smear examination of stereotaxic brain specimens. *Minim Invasive Neurosurg* 2006; 49: 353–356.
2. Bull JG, Saunders DE and Clark CA. Discrimination of paediatric brain tumours using apparent diffusion coefficient histograms. *Eur Radiol* 2012; 22: 447–457.
3. Pierce TT and Provenzale JM. Evaluation of apparent diffusion coefficient thresholds for diagnosis of medulloblastoma using diffusion-weighted imaging. *Neuroradiol J* 2014; 27: 63–74.
4. Poretti A, Meoded A and Huisman TA. Neuroimaging of pediatric posterior fossa tumors including review of the literature. *J Magn Reson Imaging* 2012; 35: 32–47.
5. Sugahara T, Korogi Y, Kochi M, et al. Usefulness of diffusion-weighted MRI with echo-planar technique in the evaluation of cellularity in gliomas. *J Magn Reson Imaging* 1999; 9: 53–60.
6. Pierce T, Kranz PG, Roth C, et al. Use of apparent diffusion coefficient values for diagnosis of pediatric posterior fossa tumors. *Neuroradiol J* 2014; 27: 233–244.
7. Rumboldt Z, Camacho DL, Lake D, et al. Apparent diffusion coefficients for differentiation of cerebellar tumors in children. *AJNR Am J Neuroradiol* 2006; 27: 1362–1369.
8. Zitouni S, Koc G, Doganay S, et al. Apparent diffusion coefficient in differentiation of pediatric posterior fossa tumors. *Jpn J Radiol* 2017; 35: 448–453.
9. Wagner MW, Narayan AK, Bosemani T, et al. Histogram analysis of diffusion tensor imaging parameters in pediatric cerebellar tumors. *J Neuroimaging* 2016; 26: 360–365.
10. Arai K, Sato N, Aoki J, et al. MR signal of the solid portion of pilocytic astrocytoma on T2-weighted images: Is it useful for differentiation from medulloblastoma? *Neuroradiology* 2006; 48: 233–237.
11. Sener RN. Diffusion MRI: Apparent diffusion coefficient (ADC) values in the normal brain and a classification of brain disorders based on ADC values. *Comput Med Imaging Graph* 2001; 25: 299–326.
12. Rodriguez Gutierrez D, Awwad A, Meijer L, et al. Metrics and textural features of MRI diffusion to improve classification of pediatric posterior fossa tumors. *AJNR Am J Neuroradiol* 2014; 35: 1009–1015.
13. Poussaint TY, Vajapeyam S, Ricci KI, et al. Apparent diffusion coefficient histogram metrics correlate with survival in diffuse intrinsic pontine glioma: A report from the Pediatric Brain Tumor Consortium. *Neuro Oncol* 2016; 18: 725–734.
14. Pope WB, Lai A, Mehta R, et al. Apparent diffusion coefficient histogram analysis stratifies progression-free survival in newly diagnosed bevacizumab-treated glioblastoma. *AJNR Am J Neuroradiol* 2011; 32: 882–889.
15. Pope WB, Qiao XJ, Kim HJ, et al. Apparent diffusion coefficient histogram analysis stratifies progression-free and overall survival in patients with recurrent GBM treated with bevacizumab: A multi-center study. *J Neurooncol* 2012; 108: 491–498.
16. Ogura A, Tamura T, Ozaki M, et al. Apparent diffusion coefficient value is not dependent on magnetic resonance systems and field strength under fixed imaging parameters in brain. *J Comput Assist Tomogr* 2015; 39: 760–765.